



Binding of MgtR, a *Salmonella* Transmembrane Regulatory Peptide, to MgtC, a *Mycobacterium tuberculosis* Virulence Factor: A Structural Study

Frantz L. Jean-Francois^{1,2}, Jian Dai^{3,4}, Lu Yu⁵, Alissa Myrick⁶, Eric Rubin⁶, Piotr G. Fajer^{1,4}, Likai Song¹, Huan-Xiang Zhou^{3,4} and Timothy A. Cross^{1,2,4}

1 - National High Magnetic Field Laboratory, Tallahassee, FL 32306, USA

2 - Department of Chemistry and Biochemistry, Florida State University, Tallahassee, FL 32306, USA

3 - Department of Physics, Florida State University, Tallahassee, FL 32306, USA

4 - Institute of Molecular Biophysics, Florida State University, Tallahassee, FL 32306, USA

5 - University of Science and Technology of China, Hefei 230031, China

6 - Department of Immunology and Infectious Diseases, Harvard School of Public Health, Boston, MA 02138, USA

Correspondence to Timothy A. Cross: National High Magnetic Field Laboratory, 1800 East Paul Dirac Drive, Tallahassee, FL 32310, USA. cross@magnet.fsu.edu

<http://dx.doi.org/10.1016/j.jmb.2013.10.014>

Edited by J. Bowie

Abstract

MgtR, a highly hydrophobic peptide expressed in *Salmonella enterica* serovar Typhimurium, inhibits growth in macrophages through binding to the membrane protein MgtC that has been identified as essential for replication in macrophages. While the *Mycobacterium tuberculosis* MgtC is highly homologous to its *S. Typhi* analogue, there does not appear to be an *Mtb* homologue for MgtR, raising significant pharmacological interest in this system. Here, solid-state NMR and EPR spectroscopy in lipid bilayer preparations were used to demonstrate the formation of a heterodimer between *S. Typhi* MgtR and the transmembrane helix 4 of *Mtb* MgtC. Based on the experimental restraints, a structural model of this heterodimer was developed using computational techniques. The result is that MgtR appears to be ideally situated in the membrane to influence the functionality of MgtC.

© 2013 Elsevier Ltd. All rights reserved.

Introduction

MgtC is an important virulence factor for pathogens that replicate in human macrophages, such as *Salmonella enterica* serovar Typhimurium (*S. Typhi*) and *Mycobacterium tuberculosis* (*Mtb*) [1,2]. It facilitates bacterial growth in low Mg²⁺ environments and is required for intramacrophage replication [3]. Recently, *S. Typhi* MgtC has been shown to inhibit the *S. Typhi* F₁F₀ ATPase through the α -subunit of the ATPase [4]. Moreover, mutations of Asn92 in the MgtC loop between transmembrane (TM) helices 3 and 4 prevent this inhibition. In *S. Typhi*, MgtR promotes the breakdown of MgtC by the FtsH protease, thereby depleting this critical virulence factor; overexpression of MgtR results in a substantial reduction in the intramacrophage growth rate [5]. Bacterial two-hybrid assays have suggested

binding between MgtR and *S. Typhi* MgtC [5]. The fact that MgtR is not found in the *Mtb* genome raises the potential of this peptide as an effector for *Mtb* replication and as a lead for drug development, if *S. Typhi* MgtR binds to *Mtb* MgtC.

MgtR consists of just 30 amino acids, with a well-defined hydrophobic sequence of 19 residues forming a putative TM helix. Recent studies have identified hydrophobic peptides as a novel class of molecules that bind to membrane proteins through van der Waals and weak electrostatic interactions [6]. Interactions between TM domains of proteins are often mediated by Ala/Ser motifs (e.g., AxxxS or AxxxxxA) instead of Gly motifs (e.g., GxxxG), which are more common for helix–helix packing within TM domains [7–10]. MgtR contains an Ala/Ser motif (bold letters) MNRSPDKIIA₁₀LIFLLISLLV₂₀LCLALWQIVF₃₀, and bacterial two-hybrid assays

showed that disruption of this motif by mutations to large hydrophobic residues prevented the interaction with *S. Typhi* MgtC [5].

Since MgtC is such an important virulence factor, there has been considerable research into the functional activities for this protein. For a long time, it was thought that MgtC had a role in Mg^{2+} transport or sequestration. However, MgtB expressed from the same operon now appears to be the Mg^{2+} transporter [11,12]. *Mtb* MgtC has 234 residues. The C-terminal half (residues 141–243), as characterized by solution NMR spectroscopy, forms a $\beta\alpha\beta\alpha\beta$ structure, similar to ACT domains that bind amino acids and/or metal ions [13]. ACT domains typically dimerize, but this C-terminal domain of MgtC does not and neither does it bind small organics or metal ions. Since there is no evidence that MgtC binds or conducts Mg^{2+} , its role in facilitating growth in low Mg^{2+} must be indirect. Mutations in MgtC (C155A and W226A) led to a substantial decrease in replication rate in low Mg^{2+} , while deletion of conserved glutamates (E160A and E209A) that might have been thought to bind Mg^{2+} had little effect [3]. In the N-terminal domain, mutations (E84A and N92T) in the cytoplasmic loop between helices 3 and 4 (TM3 and TM4 hereafter) resulted in a reduction in growth both in low Mg^{2+} and in macrophages. Mutations of residues Cys99 and Asn114 uniquely resulted in reduced growth in macrophages without a significant effect on growth in low Mg^{2+} [3].

As noted by Rang *et al.*, MgtC mutations that resulted in reduced growth in macrophages are confined to the TM N-terminal domain [3]. Interestingly, this domain has 55% sequence identity between *S. Typhi* and *Mtb*, compared to less than 20% sequence identity in the water-soluble C-terminal domain [1]. Typically, the hydrophobic residues of TM α -helical proteins facing the fatty-acyl environment of the lipid bilayer have very low sequence identity between species. Therefore, for those residues facing the interior of the MgtC TM domain, the sequence identity is likely to be even higher than 55%, further pointing to the functional importance of the TM domain.

Alix and Blanc-Potard explored potential sites of interaction in between MgtR and MgtC in *S. Typhi* [5]. Their bacterial two-hybrid assays on MgtC mutants found that mutations in the TM3–TM4 loop (E84A, G85A, and N92T) interfered with MgtR/MgtC interactions. This finding prompted Alix and Blanc-Potard to hypothesize that MgtR might interact with MgtC TM3 and/or TM4. They tested specifically an Ala/Gly motif on TM4 (Ala94, Ala101, and Gly108) and found that mutations of the first two positions to Leu had no effect (neither did the C99A mutation), but mutation of the third position to Phe did reduce the binding with MgtR. It thus appeared that this Ala/Gly motif is not the surface that directly interacts with MgtR. Instead, this motif might participate in helix–helix packing within the

MgtC TM domain, thus avoiding the exposure of a glycine on the lipid-facing surface. However, *S. Typhi* MgtC has a second potential binding motif involving Ala95 and Gly102. This latter motif is conserved in *Mtb* MgtC (first two boldfaced letters in RGL₉₀NTA **ATLWCSA**₁₀₀**AVGVLAASGH**₁₁₀LVF), with further extension of the motif to Ser108. Consequently, our hypothesis was that this motif rather than the one explored by Alix and Blanc-Potard [5] is directly responsible for MgtR binding. Moreover, in this scenario, though the Cys99 residue critical for *S. Typhi* replication is not directly in the binding interface, access to it is likely hindered by the bound MgtR, thus explaining the latter's inhibitory effect.

Protein–protein interactions mediated by Ala/Ser motifs, such as those between MgtR and MgtC TM4, are relatively weak. The resulting marginal stability for the complexes precludes classical approaches for their analysis [14–17]. Here, a solid-state NMR method called polarization inversion spin exchange at the magic angle (PISEMA) [18–22] was used to characterize the structure of a complex formed by *S. Typhi* MgtR and *Mtb* MgtC TM4. Importantly, our experimental approach permits a precise structural characterization of the polypeptide backbone in a native-like liquid crystalline lipid bilayer environment [23,24]. The anisotropic ^{15}N – ^1H dipolar couplings and anisotropic ^{15}N chemical shifts observed provide orientational restraints with respect to the external magnetic field and the bilayer normal as a result of the uniform alignment of the lipid bilayers on glass slides. These absolute structural restraints (restraints of molecular sites to a fixed frame of reference) have provided a sensitive route to determine high-resolution structures for TM helices [25,26]. In addition, site-directed spin labeling and electron paramagnetic resonance (EPR) spectroscopy [27–30] were used here for measuring a distance between the MgtR and MgtC TM helices. Using the NMR restraints, the EPR distance, as well as computational modeling [31–36], a model for this heterodimer in a DMPC bilayer was developed and refined.

Results

PISEMA data and PISA wheel analysis for MgtR

Figure 1a presents the PISEMA spectra for three specifically labeled MgtR peptides uniformly aligned in liquid crystalline DMPC lipid bilayers. These peptides, each containing four ^{15}N -labeled residues, were synthesized to allow assignment of the resonances and to characterize the PISA wheel, a wheel-like pattern of resonances imaged in PISEMA spectra of helices. This pattern permits the characterization of both the helical tilt relative to the bilayer normal and the helix rotational orientation

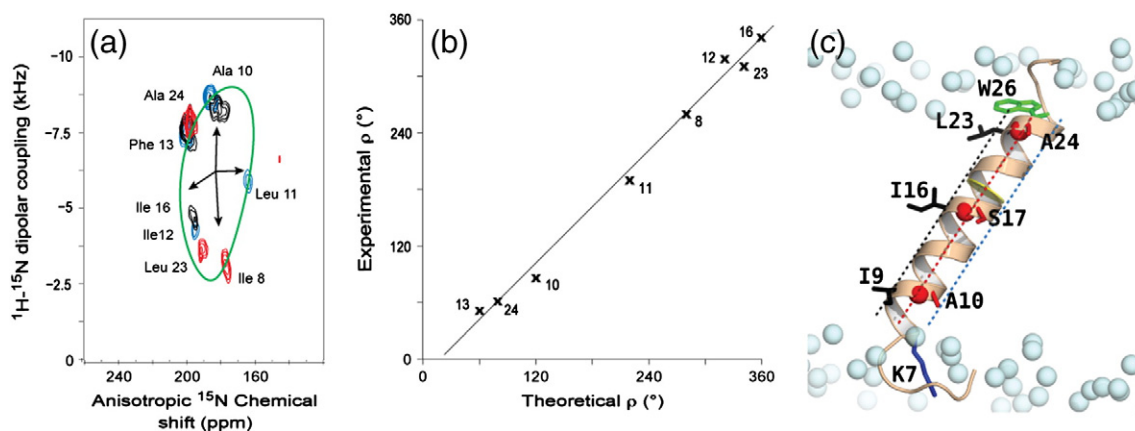


Fig. 1. (a) PISEMA spectra of MgtR selectively ^{15}N -labeled constructs in aligned DMPC bilayers. Labeled residues are as follows: construct 1, Ala10, Leu15, Ile16, and Ala24 (black); construct 2, Ala10, Leu11, Ile12, and Phe13 (blue); construct 3, Ile8, Leu23, Ala24, and Leu25 (red). The simulated 32° PISA wheel (green) is superimposed on the spectra using torsion angles of $\phi = -57^\circ$ and $\psi = -47^\circ$. (b) Experimental ρ values taken from the PISA wheel compared to theoretical values assuming an ideal helix. The linear correlation demonstrates that a uniform helix without kinks or bends extends from residue 8 to residue 24. (c) Calculated structure of MgtR in a DMPC lipid bilayer, with a 32° tilt angle. A helix cross-section (yellow) is shown to identify the top, bottom, and side of the helix. Backbone nitrogens of the Ala/Ser motif (Ala10, Ser17, and Ala24) are shown as red spheres. Side chains shown in sticks include Ala/Ser motif (red); Ile9, Ile16, and Leu23 (black); Trp26 (green); and Lys7 (blue). DMPC phosphorus atoms are shown as light-blue spheres.

[37,38]. The first peptide was ^{15}N labeled at Ala10, Leu15, Ile16, and Ala24 (black resonances in Fig. 1a), but Leu15 was not detected, possibly because the resonance would be in a region of the spectrum with broadened resonances [22,39]. The labeling scheme for this peptide was performed to identify the orientation of the Ala/Ser motif $\text{A}_{10}\text{xxxxxxS}_{17}\text{xxxxxxA}_{24}$. The second peptide was labeled at Ala10, Leu11, Ile12, and Phe13 (blue resonances in Fig. 1a) both to determine the tilt angle of the N-terminal segment of the helix and to confirm the assignment for Ala10. The purpose of synthesizing a third peptide, labeled at Ile8, Leu23, Ala24, and Leu25 (red resonances in Fig. 1a), was threefold: to confirm the assignment for Ala24, to determine the helical tilt of the C-terminal segment, and to obtain enough residue assignments to characterize the MgtR backbone structure. Once again, a resonance, this time of Leu25, at the end of the helix had low spectral intensity.

The ^{15}N resonances of the helical residues trace a PISA wheel (green solid curve in Fig. 1a), analogous to a helical wheel. The good fit to the PISA wheel at a 32° tilt angle demonstrates that a uniform α -helix is present with a uniform tilt angle (i.e., a linear helix) in these samples in liquid crystalline lipid bilayers, and it justifies the use of the uniform helical torsion angles ($\phi = -57^\circ$, $\psi = -47^\circ$) in our structural calculation with a generous error bar of $\pm 30^\circ$. The axis frame presented in Fig. 1a in the middle of the PISA wheel identifies the rotation angle ρ for the backbone nitrogens around the helical wheel. The resulting ρ values can be compared with theoretical ρ values for

a uniform helix (with 100° increment per residue) (Fig. 1b). The excellent correlation shows that the helix is uniform from residues 8 through 24. In defining the ρ angle, the top and bottom of the helical cross-section are assigned $\rho = 0^\circ$ and $\rho = 180^\circ$, respectively, as illustrated in Fig. 1c.

MgtR structure calculated from NMR restraints

Based on the PISEMA data obtained from the DMPC bilayer preparations (in particular, the uniformity of the experimental ρ values), we calculated the structure of MgtR at a 32° tilt angle (Fig. 1c). The top surface of the helix is lined by C^α atoms of Ile9, Ile16, and Leu23; the backbone nitrogens of these residues are near $\rho = 330^\circ$. The Ala/Ser motif (Ala10, Ser17, and Ala24) has its backbone nitrogens near $\rho = 75^\circ$ and its C^α atoms at approximately $\rho = 105^\circ$. The resulting relatively flat helical face, located on the side (as opposed to the top or bottom) of the helix, is optimally situated for creating an interface for binding MgtC TM4. The charged side chain of Lys7 and the indole of Trp26 of MgtR are appropriately positioned to interact with the two interfacial regions of the bilayer.

Conformation and membrane positioning of MgtR upon interaction with MgtC TM4

Figure 2 compares the PISEMA spectra of two different ^{15}N -labeled MgtR peptides, one at Ala10, Leu15, Ile16, and Ala24 and the other at Ala10,

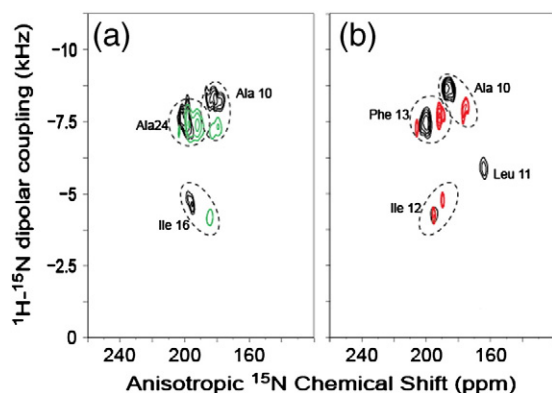


Fig. 2. PISEMA spectra of MgtR peptide in aligned DMPC bilayers with (green, red) and without (black) MgtC TM4 unlabeled peptide. (a) Construct with ^{15}N labeling at Ala10, Leu15, Ile16, and Ala24. (b) Construct with ^{15}N labeling at Ala10, Leu11, Ile12, and Phe13. Dotted circles are drawn to enclose resonances attributed to the same residue. Spectra were acquired at 310 K with 3 K scans per t_1 increment.

Leu11, Ile12, and Phe13, with and without unlabeled MgtC TM4. The resonances of MgtR showed discernible shifts in the presence of MgtC TM4, indicating a binding interaction between these two peptides. For the second labeled MgtR peptide, the resonance of Leu11 in the presence of MgtC TM4 was not detectable, again likely falling in the region of the spectrum where resonances are potentially broadened. While the changes in anisotropic chemical shifts and dipolar couplings (up to 13 ppm and 1.25 kHz, respectively) are certainly above experimental errors, they do not indicate substantial changes in the tilt or rotation of the MgtR helix and could be attributed to small conformational and/or dynamical differences upon complex formation. The spectrum of the second labeled MgtR sample with MgtC TM4 (Fig. 2b) showed doubling of some resonances, suggesting incomplete saturation of MgtR by MgtC. The frequency difference between bound and unbound states places an upper limit of ~ 1 kHz on the exchange rate.

MgtC TM4 tilt angle revealed by solid-state NMR data

Figure 3 shows a superposition of the ^{15}N one-dimensional cross-polarization spectra of MgtC TM4 with and without unlabeled MgtR. Akin to the labeling strategy used for MgtR, four ^{15}N -labeled residues were introduced into the MgtC TM4 sequence: Ala93, Ala94, Ala107, and Val102. The spectral dispersion was insufficient to distinguish the four resonances in the one-dimensional spectra. However, the anticipated spectral dispersion around the PISA wheel for these four resonances, assuming

an ideal helix, spans nearly the full range of the anisotropic chemical shifts attributable to the four labeled residues. Assuming $\rho = 0^\circ$ for Ala93 and 100° increments per residue for Ala94, Ala107, and Val102, the minimum and maximum anisotropic chemical shifts for these four residues can be estimated from the observed signals and are illustrated by the vertical black lines in Fig. 3. Comparing the calculated PISA wheels for 17° , 19° , and 21° tilt angles, an approximate tilt angle of $19 \pm 2^\circ$ is consistent with the experimental data. It is clear from the overlay of the spectra that the helical tilt angle of MgtC TM4 does not change significantly upon binding MgtR.

EPR evidence for the presence of homodimers and heterodimers

To further investigate the association of MgtC TM4 with MgtR, we used the unique native cysteine sites in MgtR and MgtC TM4 (residues 22 and 98, respectively) and attached a nitroxide spin label (MTSSL). The possibility of homodimerization was assessed by recording the EPR spectra of each individually labeled peptide in DMPC liposomes and a corresponding sample with 30% labeling (Fig. 4a and b). Each 30% labeled sample was prepared by mixing the labeled peptide with the Cys-to-Ser mutant peptide. We then recorded the EPR spectrum of a sample with labeled MgtR and labeled MgtC TM4 peptides reconstituted together in DMPC liposomes (red curve in Fig. 4c). Possible formation of homodimers and heterodimers in this sample was assessed by comparing its EPR spectrum to the sum of the spectra of two samples with singly labeled peptides (labeled MgtR mixed with MgtC TM4 Cys-to-Ser mutant or MgtR Cys-to-Ser mutant mixed with labeled MgtC TM4; black curve in Fig. 4c). In all three cases, the fully labeled samples relative to the samples with reduced labeling show a small but clear decrease in spectral intensity. This decrease indicates a broadening of the EPR lineshape, and hence, the presence of spin-spin interactions within 25 \AA (Fig. S1). The broadening was deconvoluted to yield spin-spin distances of $16 \pm 1 \text{ \AA}$ for pure MgtR, $13.5 \pm 1 \text{ \AA}$ for pure MgtC TM4, and $9 \pm 1 \text{ \AA}$ for the mixture of MgtR and MgtC TM4. The EPR results show that MgtR and MgtC TM4 form homodimers individually and confirm that they form a heterodimer when mixed together.

Structural model for the MgtR/MgtC TM4 heterodimer in a DMPC bilayer

Based on the calculated structure (along with its helix tilt and rotation) for MgtR from the NMR restraints, the observed tilt angle of MgtC TM4, and the expectation that the Ala/Ser motif of MgtR is buried in the dimer interface, we used RosettaDock

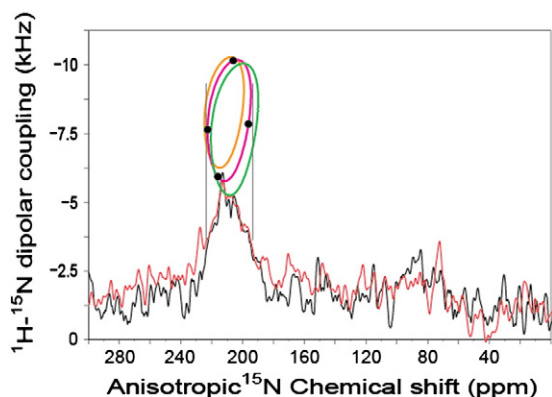


Fig. 3. One-dimensional anisotropic ^{15}N chemical shift spectra of MgtC TM4 in aligned DMPC bilayers with (red) and without (black) unlabeled MgtR. Spectra were acquired at 310 K with 3 K scans per t_1 increment. Black vertical lines reflect an estimate for the limits of the chemical shift dispersion for the four resonance frequencies. Simulated PISA wheels predict a dispersion of chemical shifts for ideal helices having a tilt of 17° (orange), 19° (magenta), and 21° (green). The black dots on the 19° PISA wheel illustrate the distribution of resonances for Ala93, Ala94, Val102, and Ala107 assuming rotational angles of 0° , 100° , 180° , and 320° in an ideal helix. Similar dispersion of these resonances on the PISA wheel is obtained if a different helical rotation is assumed.

to generate 4827 models for the MgtR/MgtC TM4 heterodimer [35,40,41]. A scatter plot of their interface scores *versus* root-mean-square-deviations from a seed with low interface score is shown in Fig. 5a. Two clusters with low interface scores can be identified: a major cluster containing 300 models (lowest score = -6.6) and a minor cluster containing 13 models (lowest score = -7.6). Both clusters represent a parallel configuration for the two helices, with a left-handed crossing angle of approximately 16° for the major cluster and of 19° for the minor cluster. A striking feature of these two sets of models is that different Ala/Ser motifs of MgtC TM4 are placed at approximately the same position in the interface with MgtR (Fig. 5b). In the major cluster, the Ala/Ser motif of MgtC TM4 consists of Ala94, Ala101, and Ser108 (Fig. 5c), while in the minor cluster, the motif consists of Ala93, Ala100, and Ala107 (Fig. 5d).

Both clusters of models can satisfy the spin–spin distance of $9 \pm 1 \text{ \AA}$ measured in the EPR experiment (Fig. S2). To satisfy the EPR distance restraint between the spin label O1 atoms, the spin labels have to be oriented with the O1 atoms much closer to each other than the C^α atoms, which are nearly 20 \AA apart in both of these clusters (Fig. S2b and d). In addition, the O1 atoms have to be close to the surfaces of the helices (Fig. S2a and c). This is especially true for the major cluster since, in this case, the C^α atoms to which the spin labels are

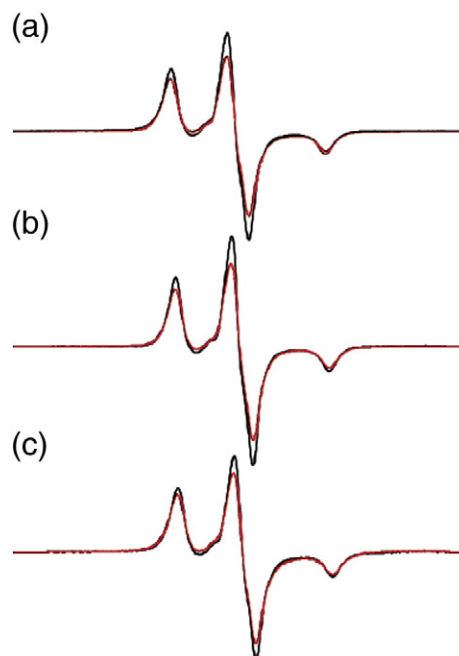


Fig. 4. EPR spectra of MgtR and MgtC TM4 reconstituted in DMPC liposomes. (a) MgtR; (b) MgtC TM4; and (c) MgtR/MgtC TM4 mixture. Red curves display the spectra of fully labeled peptides. Black curves display controls using 30% labeled peptides in (a) and (b) and the sum of singly labeled peptides in (c). Broadening of the red spectra indicates spin–spin coupling within 25 \AA .

attached are located on opposite faces of the MgtR/MgtC TM4 dimer (Fig. S2a).

Because of the significantly larger cluster size and other considerations (see Discussion), we propose that the major cluster represents the physical interaction between MgtR and MgtC TM4. We further refined a model from this cluster by a restrained molecular dynamics (MD) simulation in the DMPC bilayer. The restraints include the PISEMA data on MgtR, the experimental tilt angle of MgtC TM4, and the EPR spin–spin distance (after adding the two spin labels to the model). This model is shown in Fig. 6a. The helix–helix interface is very well packed (Fig. 6b). Furthermore, the two spin labels fit snugly into crevices, one over the helix–helix interface and the other one on the external side of MgtR (Fig. S3).

Discussion

The length of the interaction surface between two tilted TM helices is maximized when they have a parallel (or antiparallel), side-by-side arrangement. In this optimal situation, the interfacial residues are positioned on the side, as opposed to the top or bottom, of each helix (see illustration in Fig. 1c). Based on high-resolution orientational restraints, the C^α atoms of the MgtR Ala/Ser motif are positioned at

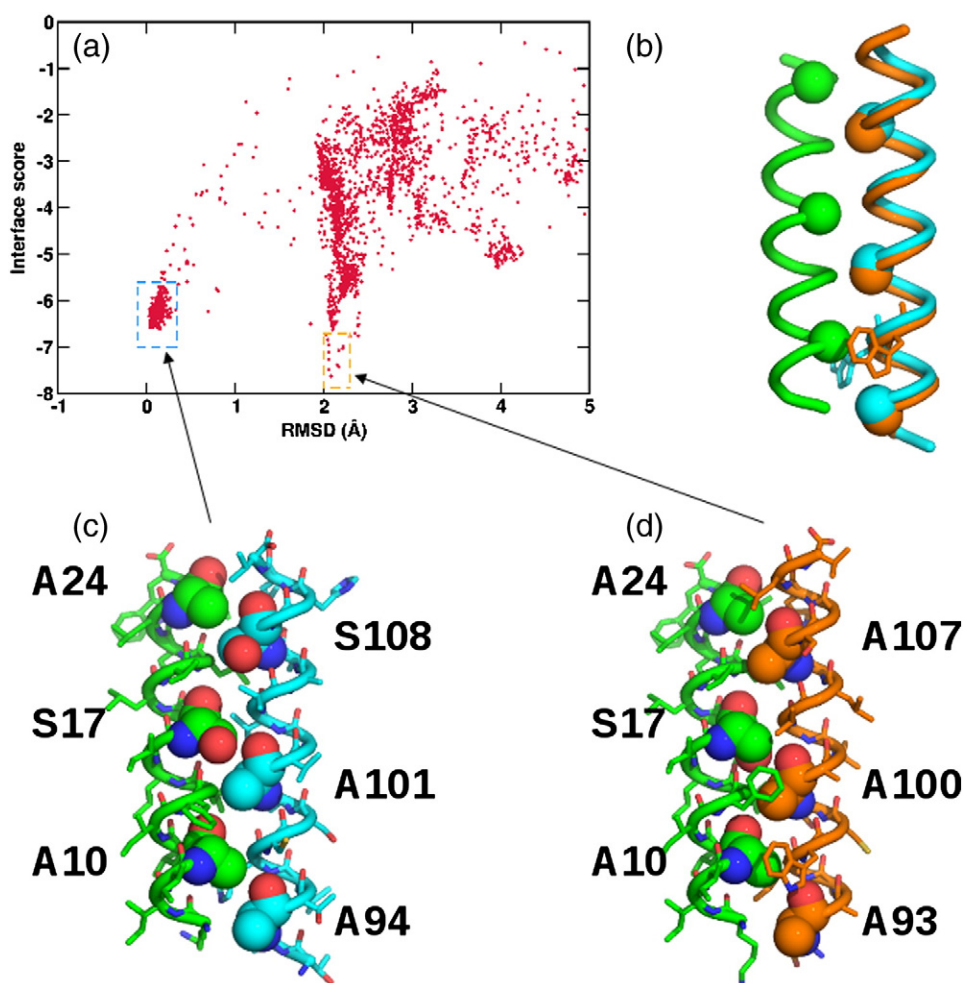


Fig. 5. Structural models of the MgtR/MgtC TM4 dimer generated by RosettaDock. (a) Scatter plot of interface scores *versus* root-mean-square-deviations from a seed model with low interface score. Two low-score clusters, with 300 and 13 poses, respectively, are highlighted in cyan and orange boxes. (b) Conformations of the two clusters. The green helix is MgtR, and the cyan and orange helices are MgtC TM4 in the major and minor clusters, respectively. The C α atoms of the Ala/Ser motifs of MgtR and MgtC TM4 are shown as spheres. Trp97 of MgtC TM4 is shown as sticks in order to assist in locating the position and orientation of this peptide. Models of (c) the major cluster and (d) the minor cluster. Ala/Ser motif residues are shown as spheres; other residues are shown as sticks.

approximately $\rho = 105^\circ$, close to the optimal location. Moreover, the tilt angles of MgtR and *Mtb* MgtC TM4 have been determined at 32° and 19° , respectively. These values for the tilt angles suggest that the two helices can easily adopt a nearly parallel arrangement. The MgtR Ala/Ser motif has been implicated in interactions with *S. Typhi* MgtC by the mutational study of Alix and Blanc-Potard [5]. It now appears that this motif is nearly optimally positioned for these interactions.

The presence of homodimers is not surprising given that an Ala/Ser motif is the hallmark of TM helix-helix interactions. Both MgtR and MgtC TM4 contain Ala/Ser motifs, and therefore, dimerization is likely between these two helices. EPR data confirmed the presence of both homodimers and heterodimers in liposomes containing either one or

both of MgtR and MgtC TM4 peptides. The topology of MgtC [3], the positive inside rule [42], and the mutational results of Alix and Blanc-Potard [5] all suggest that MgtC is oriented in the cytoplasmic membrane such that the N-terminus of TM4 is on the cytoplasmic side. Similarly, the positive inside rule suggests that the positively charged N-terminus of MgtR is on the cytoplasmic side, leading to a parallel configuration for the MgtC TM4 and MgtR helices, just as we found in DMPC bilayers.

The *Mtb* MgtC TM4 sequence contains two Ala/Ser motifs: one consists of Ala93, Ala100, and Ala107; the other, shifted by 100° in ρ , consists of Ala94, Ala101, and Ser108. The two low-energy clusters from the RosettaDock modeling involve the two different Ala/Ser motifs. The number of models (13 *versus* 300) in each cluster shows a

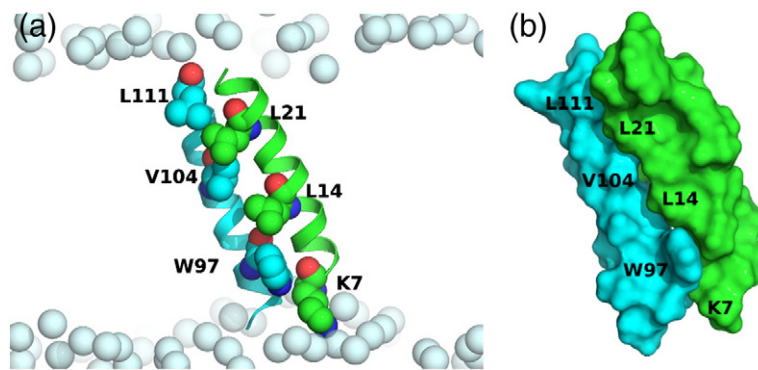


Fig. 6. Structural model of the MgtR/MgtC TM4 dimer refined by MD simulation in the DMPC bilayer. MgtR and MgtC TM4 are represented in green and cyan, respectively. (a) Positioning of the dimer in the DMPC bilayer. Each peptide is shown as a helix, with three residues are shown as van der Waals spheres. DMPC phosphorus atoms are shown as light-blue spheres. (b) Representation of the dimer by van der Waals surface, illustrating the snug fit in the interface.

considerable preference for interactions involving the second of these motifs. Projection of the MgtC TM4 side chains on the helical wheel shows that only the second Ala/Ser motif forms a flat helical face (Fig. S4), allowing for optimal packing against the flat face of the MgtR helix lined by the latter's own Ala/Ser motif.

Figure 5c and d shows that the MgtR and MgtC Ala/Ser motifs are not in direct interaction with one another despite facing each other. There is a slight shift along the helical axis that creates an efficient interdigitation of the Ala/Ser motif side chains from the two helices in the interface. According to Senes *et al.*, for membrane proteins having small side chains every four or seven residues, helix-helix interactions in the membrane may be stabilized in part by hydrogen bonds that occur between C^αH and either the backbone carbonyl oxygens or hydroxyl oxygens from side chains [43]. In addition, the close approach of the two helices may permit much greater van der Waals interactions between the two helices. In our structural model for the MgtR/MgtC TM4 dimer, bulky residues Lys7, Leu14, and Leu21 on MgtR and Trp97, Val104, and Leu111 on MgtC TM4 are present in the interaction region, generating a large interdigitated van der Waals interface between the two helices (Fig. 6b). These two helices have highly complementary surfaces in which large residues on MgtR pair with small residues on MgtC TM4 and vice versa: Lys7 with Ala94, Ala10 with Trp97, Leu14 with Ala101, Ser17 with Val104, Leu21 with Ser108, and Ala24 with Leu111. Consequently, our structural model for the MgtR/MgtC TM4 dimer conforms to the notion that the specificity of TM peptide interactions can be mainly driven by efficient packing of side chains referred to as “knobs into holes” [44,45]. Furthermore, the helix-helix packing in our model positions MgtR Ser17 and MgtC Ser108 at the dimer interface, which could further stabilize the dimer via potential C^αH–O hydrogen bonds.

The structural model shows that the interaction surface spans the entire TM domain as a result of the small crossing angle of 16°. The positioning of the entire MgtR Ala/Ser motif in the interface is in agreement with the study of Alix and Blanc-Potard [5] showing that the mutation of any of the three residues in the motif to a large hydrophobic residue prevented the interaction with *S. Typhi* MgtC. The same study also found that Leu mutations of *S. Typhi* MgtC residues corresponding to the first two positions of the first Ala motif of *Mtb* MgtC TM4 had no effect, though a G108F mutation in the third position reduced the binding with MgtR. These mutational results are consistent with our placement of the second Ala/Ser motif of *Mtb* MgtC TM4 in the interface with MgtR. The first Ala motif of MgtC TM4 could be involved in tertiary interactions, interfacing with one of the other four TM helices of MgtC. The minor effect of the *S. Typhi* MgtC G108F mutation observed by Alix and Blanc-Potard can be explained if the bulky Phe side chain interferes with MgtR binding.

If as just suggested the first Ala motif, consisting of residues 93, 100, and 107, on MgtC TM4 forms an interface with another MgtC TM helix, then Cys98, which is in the middle of TM4, is on the opposite side from this motif (Fig. S4) and may be exposed to the fatty-acyl environment. The counterpart of Cys98 in *S. Typhi* MgtC has been shown to be essential for intramacrophage replication. Previously, it has been suggested that this residue might form a disulfide bond within MgtC or between MgtC and an unknown partner [5]. If indeed Cys98 faces the fatty-acyl environment, then it is unlikely to be able to form a disulfide bond within MgtC. In addition, according to our model for the MgtR/MgtC TM4 complex, the C^α atoms of MgtC Cys98 and MgtR Cys22 are 18.2 Å apart, making a disulfide bond with MgtR impossible. However, because Cys98 is close to the Ala/Ser motif that MgtR binds to, it is possible that MgtR prevents the functional activity associated with Cys98 by hindering access to this residue by other partners.

Recently, the importance of another residue Asn92 (in *S. Typhi* corresponding to Asn91 in *Mtb* MgtC) was accentuated when it was discovered that this residue was essential for the MgtC inhibition of the F_1F_0 ATPase [4]. This Asn site is within three residues of the start of the MgtC TM4 helix, and the hydrophilic N-terminal segment (seven residues) of MgtR is long enough to reach this critical MgtC residue, suggesting that MgtR might interfere with this inhibitory effect of MgtC.

Conclusions

In this study, we have set out to explore the potential to influence the virulence activities of *Mtb* MgtC with *S. Typhi* MgtR. In *S. Typhi*, MgtR is known to induce the degradation of MgtC, a protein that is essential for bacterial replication in macrophages [5]. Moreover, in *S. Typhi*, the conserved Asn92 is essential for MgtC inhibition of the F_1F_0 ATPase [4] and the conserved Cys99 is critical for intramacrophage replication [3]. Here, we have shown that *S. Typhi* MgtR binds to the TM4 helix of *Mtb* MgtC. The structural model of the complex is supported by numerous experimental restraints, all of which have been obtained from a native-like lipid environment. This model suggests how *S. Typhi* MgtR might interfere with the functional and virulence activity at both Cys98 and Asn91 residues in *Mtb* MgtC. Hydrophobic peptides such as MgtR are being recognized as novel regulators of membrane proteins [6], and as with antimicrobial peptides that have been used as drugs [46,47], MgtR could represent a lead compound as an effector of *Mtb* replication in macrophages, potentially opening a new approach for tuberculosis drug development.

Experimental and Computational Methods

Peptide synthesis

Fmoc-Phe-Novasyn TGA 2-(1*H*-benzotriazole-1-yl)-1,1,3,3-tetramethyl-uronium and N- α -Fmoc-amino acids were purchased from VWR-NovaBiochem (Hohenbrunn, Germany). Amino acids were protected by *t*-butyl for serine and tyrosine and by 2,2,4,6,7-pentamethyl-dihydrobenzofuran-5-sulfonyl for arginine. The syntheses were performed on an Applied Biosystems 433A Peptide Synthesizer, using Fmoc strategy [48]. The resins were preloaded with phenylalanine substituted at 0.21 mmol/g on a Novasyn TGA.

Solid-state NMR spectroscopy

Aligned lipid bilayer samples containing both peptides were prepared using 4 mg of MgtR and/or

3 mg of MgtC TM4 cosolubilized in 5 ml buffer (2.3% sodium dodecyl sulfate, 10 mM β -mercaptoethanol, and 20 mM Tris-HCl, pH 8.0). We solubilized 70 mg of DMPC lipids (Avanti Polar Lipids) in 4 ml of the same buffer. The two solutions were mixed and incubated at 37 °C. The preparation was dialyzed for 4 days in a dialysis bag with a 3-kDa molecular mass cutoff against 20 mM Tris-HCl buffer (pH 8.0) containing methyl β -cyclodextrin at double the molar ratio of SDS. The proteoliposomes were pelleted at 196,000g, and the oriented samples were prepared as described in the supplemental information and similar to the protocol in Das *et al.* [49]. NMR experiments were performed in a 400-MHz spectrometer at 37 °C using a home-built low-E static NMR probe [50]. A ^1H RF field strength of 50 kHz for the 800- μs cross-polarization and 62.5 kHz for decoupling were used for PISEMA experiments; 4000 scans were acquired for each of the 32 t_1 increments. The ^{15}N chemical shift was referenced to a saturated solution of ammonium sulfate signal at 26 ppm.

To simulate PISA wheels, we used an average ^{15}N - ^1H dipolar magnitude ($\nu_{\parallel} = 10.735$ kHz) and ^{15}N chemical shift tensor elements ($\delta_{11} = 57$, $\delta_{22} = 81$, and $\delta_{33} = 228$ ppm) [38,51,52]. PISA wheels were calculated for a helix at various tilt angles with respect to the bilayer normal, using uniform backbone torsion angles ($\phi = -57^\circ$, $\psi = -47^\circ$) [53,54].

Continuous wave EPR spectroscopy

Native cysteines in MgtR and *Mtb* MgtC TM4 (residues 22 and 98, respectively) were spin-labeled. Purified MgtR and MgtC TM4 were solubilized at 100 μM in methanol and dimethylformamide, respectively, and then incubated with 8-fold molar excess of the MTSSL [*S*-(2,2,5,5-tetramethyl-2,5-dihydro-1*H*-pyrrol-3-yl)methyl methanesulfonothioate] spin label at 4 °C overnight. The organic solvents were subsequently evaporated, and the powders were resuspended in 2% aqueous SDS. The excess unbound spin labels were diluted (1/2000) by dialysis (3-kDa dialysis bag) against a Tris-HCl (pH 8.0) buffer containing 2% SDS. As above, the peptide was transferred to DMPC liposomes. The proteoliposome concentrations were adjusted to obtain 80 μl of 200–300 μM peptides, and four freeze-thaw cycles were applied to assure homogeneity. The sample was made 40% in glycerol for cryoprotection. Continuous wave EPR measurements were performed on a Bruker ELEXSYS E680 spectrometer (Bruker Biospin, Billerica, MA) at 150 K with 9.6 GHz microwave frequency and 0.2 mW microwave power, 1 Gauss modulation amplitude, 100 kHz modulation frequency, and 1024 acquisition points within a 200-G field sweep. EPR spectra were analyzed with a Monte Carlo/Simplex Gaussian convolution method to extract the spin-spin distance [55].

The EPR data provided an estimate of the distance between two oxygen (O1) atoms at the tip of the MTSSL spin labels, which was transformed to an estimate for the distance between the C α atoms of the two spin-labeled cysteine residues. Following Finiguerra *et al.* [56], we approximated the position of the tip of the label that gave rise to the EPR signal as being within a hemisphere of 9 Å radius centered at the cysteine C α carbon. The EPR distance restraint was considered satisfied if the C α positions of the label cysteines and the axes of the two helices were such that, at least one pair of points, one within each hemisphere was at the measured spin–spin distance (i.e., 9 ± 1 Å).

MgtR structural calculation

For MgtR, the PISEMA restraints and the helical restraints from the PISA wheel analysis (Table S1) were used in Xplor-NIH [57] to generate structural models following the protocol of Sharma *et al.* [21]. Simulated annealing was then conducted following the details given in the supplemental material similar to the protocol of Sharma *et al.* [21]. The resulting conformation was subjected to 1000 steps of energy minimization. Finally, an average structure was generated using the top 50 of the 100 models. The average structure was embedded in a DMPC bilayer, and the side-chain conformations in the membrane environment were refined through an MD simulation. Lipid and water molecules that overlapped with the MgtR molecule were removed, and 11 Na $^+$ and 12 Cl $^-$ ions were added to neutralize the system. Prior to the MD simulation, the system was energy minimized while fixing the peptide backbone. During the simulation, the C α carbons of residues 7–26 (the TM helix) were restrained. The simulation was at constant temperature (310 K) and pressure (1 atm) and lasted 4.7 ns. The CHARMM27 force field [58] was used.

Docking of MgtR and MgtC TM4

RosettaDock [35,40,41] was used to model the heterodimer interface between the MgtR and MgtC TM4 helices. MgtR (with structure from the end of the MD simulation in the DMPC bilayer) was fixed while MgtC TM4 (built as an ideal helix) was free to translate and rotate. Two consecutive global docking steps were employed, both in the Ala/Ser motif (Ala10, Ser17, and Ala24) of MgtR were restrained to the interface [5] with MgtC TM4. The first docking step started from an arbitrarily positioned MgtC TM4. Out of 89,662 poses, 10,260 in which the tilt angle of MgtC TM4 agreed with the NMR value of $19 \pm 2^\circ$ were selected. The pose with a low interface score was chosen to seed the second docking step. Out of 29,704 poses generated, 4827 passed the tilt angle filter.

Refinement of the MgtR/MgtC TM4 structural model

A dimer model in the low-score major cluster of the second docking step was further refined by restrained MD simulation in a DMPC bilayer. To enforce the EPR distance restraint, we mutated the Cys residues to MTSSL. The topology and corresponding CHARMM force field parameters for MTSSL were from Sale *et al.* [59]. First, the dimer with the MTSSL labels was energy minimized for 10,000 steps, while restraining the backbone atoms with a force constant of 1 kcal/mol/Å 2 . Second, the system temperature was ramped up from 310 K to 1000 K with an increment of 10 K. Third, the system temperature was ramped down from 1000 K to 310 K. The distance of the O1 atoms of the two spin labels was restrained by a harmonic potential with a target value of 8 Å and a force constant of 30 kcal/mol/Å 2 . The final O1–O1 distance was 9.4 Å.

The heterodimer was then embedded in the DMPC bilayer as described for the MgtR-only simulation. The whole system was equilibrated for 20 ns, while restraining the backbone atoms with a force constant of 1 kcal/mol/Å 2 and the distance of the O1–O1 distance with a force constant of 30 kcal/mol/Å 2 .

To prepare for the introduction of the PISEMA restraints, we further simulated the system for 1 ns using a new set of restraints, with the time step now reduced from 2 fs to 1 fs. The restraints included those on the C α atoms (force constant = 1 kcal/mol/Å 2), backbone torsion angles of MgtR (to ideal value with force constant = 100 kcal/mol/rad 2), i to $i + 4$ hydrogen bonds in MgtR (force constant = 10 kcal/mol/Å 2), tilt angle of MgtC TM4 (to 21° with force constant = 50 kcal/mol/deg 2 , through using the *orientation-angle* collective variable module in NAMD [60]), and O1–O1 distance (force constant = 30 kcal/mol/Å 2).

Finally, the PISEMA restraints (Table S1) were introduced on MgtR by ramping up the force constants from 0 to 1 kcal/mol/kHz 2 for dipolar couplings and from 0 to 0.02 kcal/mol/ppm 2 for the anisotropic chemical shifts over a period of 1 ns, following Sharma *et al.* [21]. The simulation was continued for another 3 ns with the force constants for the PISEMA restraints kept at their final values, the restraints on the MgtR backbone torsion angles and hydrogen bonds removed, and all the other restraints maintained.

Accession numbers

Coordinates, restraints, and so on have been deposited in the Protein Data Bank with accession code 2mc7 and in the Biological Magnetic Resonance Data Bank with accession number 19430.

Acknowledgements

We gratefully thank Huajun Qin and Umesh Goli (Department of Chemistry and Biochemistry, Florida State University, Tallahassee, FL 32306) for their help in molecular biology and peptide purification and mass spectrometry analyses. This work was supported by the National Institutes of Health Grants AI074805 and GM088187. The NMR experiments were performed at the National High Magnetic Field Laboratory supported by cooperative agreement (DMR-1157490) with the State of Florida.

Appendix A. Supplementary data

Supplemental information includes further details for the experimental and computational methods as well as four additional figures. Supplementary data associated with this article can be found, in the online version, at <http://dx.doi.org/10.1016/j.jmb.2013.10.014>.

Received 20 August 2013;

Received in revised form 10 October 2013;

Accepted 11 October 2013

Available online 17 October 2013

Keywords:

solid-state nuclear magnetic resonance;
electron spin resonance;
restrained molecular dynamics;
orientational restraints;
distance restraints

Abbreviations used:

PISEMA, polarization inversion spin exchange at the magic angle; MD, molecular dynamics.

References

- [1] Buchmeier N, Blanc-Potard A, Ehrt S, Piddington D, Riley L, Groisman EA. A parallel intraphagosomal survival strategy shared by *Mycobacterium tuberculosis* and *Salmonella enterica*. *Mol Microbiol* 2000;35:1375–82.
- [2] Blanc-Potard AB, Groisman EA. The *Salmonella selC* locus contains a pathogenicity island mediating intramacrophage survival. *EMBO J* 1997;16:5376–85.
- [3] Rang C, Alix E, Felix C, Heitz A, Tasse L, Blanc-Potard AB. Dual role of the MgtC virulence factor in host and non-host environments. *Mol Microbiol* 2007;63:605–22.
- [4] Lee EJ, Pontes MH, Groisman EA. A bacterial virulence protein promotes pathogenicity by inhibiting the bacterium's own F₁F₀ ATP synthase. *Cell* 2013;154:146–56.
- [5] Alix E, Blanc-Potard AB. Peptide-assisted degradation of the *Salmonella* MgtC virulence factor. *EMBO J* 2008;27:546–57.
- [6] Alix E, Blanc-Potard AB. Hydrophobic peptides: novel regulators within bacterial membrane. *Mol Microbiol* 2009;72:5–11.
- [7] Dong H, Sharma M, Zhou HX, Cross TA. Glycines: role in alpha-helical membrane protein structures and a potential indicator of native conformation. *Biochemistry* 2012;51:4779–89.
- [8] Lemmon MA, Flanagan JM, Treutlein HR, Zhang J, Engelman DM. Sequence specificity in the dimerization of transmembrane alpha-helices. *Biochemistry* 1992;31:12719–25.
- [9] Senes A, Engel DE, DeGrado WF. Folding of helical membrane proteins: the role of polar, GxxxG-like and proline motifs. *Curr Opin Struct Biol* 2004;14:465–79.
- [10] Senes A, Gerstein M, Engelman DM. Statistical analysis of amino acid patterns in transmembrane helices: the GxxxG motif occurs frequently and in association with beta-branched residues at neighboring positions. *J Mol Biol* 2000;296:921–36.
- [11] Gunzel D, Kucharski LM, Kehres DG, Romero MF, Maguire ME. The MgtC virulence factor of *Salmonella enterica* serovar Typhimurium activates Na(+), K(+)-ATPase. *J Bacteriol* 2006;188:5586–94.
- [12] Snavely MD, Miller CG, Maguire ME. The *mgtB* Mg²⁺ transport locus of *Salmonella typhimurium* encodes a P-type ATPase. *J Biol Chem* 1991;266:815–23.
- [13] Yang Y, Labesse G, Carrere-Kremer S, Esteves K, Kremer L, Cohen-Gonsaud M, et al. The C-terminal domain of the virulence factor MgtC is a divergent ACT domain. *J Bacteriol* 2012;194:6255–63.
- [14] Buffy JJ, Waring AJ, Hong M. Determination of peptide oligomerization in lipid bilayers using 19 F spin diffusion NMR. *J Am Chem Soc* 2005;127:4477–83.
- [15] Hou G, Yan S, Sun S, Han Y, Byeon IJ, Ahn J, et al. Spin diffusion driven by R-symmetry sequences: applications to homonuclear correlation spectroscopy in MAS NMR of biological and organic solids. *J Am Chem Soc* 2011;133:3943–53.
- [16] Mani R, Cady SD, Tang M, Waring AJ, Lehrer RI, Hong M. Membrane-dependent oligomeric structure and pore formation of a beta-hairpin antimicrobial peptide in lipid bilayers from solid-state NMR. *Proc Natl Acad Sci USA* 2006;103:16242–7.
- [17] Marulanda D, Tasayco ML, Cataldi M, Arriaran V, Polenova T. Resonance assignments and secondary structure analysis of *E. coli* thioredoxin by magic angle spinning solid-state NMR spectroscopy. *J Phys Chem B* 2005;109:18135–45.
- [18] De Angelis AA, Nevzorov AA, Park SH, Howell SC, Mrse AA, Opella SJ. High-resolution NMR spectroscopy of membrane proteins in aligned bicelles. *J Am Chem Soc* 2004;126:15340–1.
- [19] Nishimura K, Kim S, Zhang L, Cross TA. The closed state of a H⁺ channel helical bundle: combining precise orientational and distance restraints from solid state NMR. *Biochemistry* 2002;41:13170–7.
- [20] Park SH, De Angelis AA, Nevzorov AA, Wu CH, Opella SJ. Three-dimensional structure of the transmembrane domain of Vpu from HIV-1 in aligned phospholipid bicelles. *Biophys J* 2006;91:3032–42.
- [21] Sharma M, Yi M, Dong H, Qin H, Peterson E, Busath DD, et al. Insight into the mechanism of the influenza A proton channel from a structure in a lipid bilayer. *Science* 2010;330:509–12.
- [22] Verardi R, Shi L, Traaseth NJ, Walsh N, Veglia G. Structural topology of phospholamban pentamer in lipid bilayers by a hybrid solution and solid-state NMR method. *Proc Natl Acad Sci USA* 2011;108:9101–6.

- [23] Zhou HX, Cross TA. Modeling the membrane environment has implications for membrane protein structure and function: influenza A M2 protein. *Protein Sci* 2013;22:381–94.
- [24] Zhou HX, Cross TA. Influences of membrane mimetic environments on membrane protein structures. *Annu Rev Biophys* 2013;42:361–92.
- [25] Kim S, Quine JR, Cross TA. Complete cross-validation and *R*-factor calculation of a solid-state NMR derived structure. *J Am Chem Soc* 2001;123:7292–8.
- [26] Murray DT, Das N, Cross TA. Solid state NMR strategy for characterizing native membrane protein structures. *Acc Chem Res* 2013;46:2172–81.
- [27] Cortes DM, Cuello LG, Perozo E. Molecular architecture of full-length KcsA: role of cytoplasmic domains in ion permeation and activation gating. *J Gen Physiol* 2001;117:165–80.
- [28] Jennings-Antipov LD, Song L, Collier RJ. Interactions of anthrax lethal factor with protective antigen defined by site-directed spin labeling. *Proc Natl Acad Sci USA* 2011;108:1868–73.
- [29] Rabenstein MD, Shin YK. Determination of the distance between two spin labels attached to a macromolecule. *Proc Natl Acad Sci USA* 1995;92:8239–43.
- [30] Scarpelli F, Drescher M, Rutters-Mejneke T, Holt A, Rijkers DT, Killian JA, et al. Aggregation of transmembrane peptides studied by spin-label EPR. *J Phys Chem B* 2009;113:12257–64.
- [31] Psachoulia E, Marshall DP, Sansom MS. Molecular dynamics simulations of the dimerization of transmembrane alpha-helices. *Acc Chem Res* 2010;43:388–96.
- [32] Adams P, Arkin I, Engelman D, Brunger A. Computational searching and mutagenesis suggest a structure for the pentameric transmembrane domain of phospholamban. *Nat Struct Biol* 1995;2:154–62.
- [33] Fleishman SJ, Schlessinger J, Ben-Tal N. A putative molecular-activation switch in the transmembrane domain of erbB2. *Proc Natl Acad Sci USA* 2002;99:15937–40.
- [34] Zhu J, Luo BH, Barth P, Schonbrun J, Baker D, Springer TA. The structure of a receptor with two associating transmembrane domains on the cell surface: integrin alphaIIb beta3. *Mol Cell* 2009;34:234–49.
- [35] Wang C, Bradley P, Baker D. Protein–protein docking with backbone flexibility. *J Mol Biol* 2007;373:503–19.
- [36] MacKenzie KR, Prestegard JH, Engelman DM. A transmembrane helix dimer: structure and implications. *Science* 1997;276:131–3.
- [37] Marassi FM, Opella SJ. A solid-state NMR index of helical membrane protein structure and topology. *J Magn Reson* 2000;144:150–5.
- [38] Wang J, Denny J, Tian C, Kim S, Mo Y, Kovacs F, et al. Imaging membrane protein helical wheels. *J Magn Reson* 2000;144:162–7.
- [39] Quine JR, Achuthan S, Asbury T, Bertram R, Chapman MS, Hu J, et al. Intensity and mosaic spread analysis from PISEMA tensors in solid-state NMR. *J Magn Reson* 2006;179:190–8.
- [40] Barth P, Schonbrun J, Baker D. Toward high-resolution prediction and design of transmembrane helical protein structures. *Proc Natl Acad Sci USA* 2007;104:15682–7.
- [41] Chaudhury S, Berrondo M, Weitzner BD, Muthu P, Bergman H, Gray JJ. Benchmarking and analysis of protein docking performance in Rosetta v3.2. *PLoS One* 2011;6:e22477.
- [42] von Heijne G. Membrane protein structure prediction. Hydrophobicity analysis and the positive-inside rule. *J Mol Biol* 1992;225:487–94.
- [43] Senes A, Ubarretxena-Belandia I, Engelman DM. The Calpha—H...O hydrogen bond: a determinant of stability and specificity in transmembrane helix interactions. *Proc Natl Acad Sci USA* 2001;98:9056–61.
- [44] Crick FHC. The packing of alpha-helices: simple coiled coils. *Acta Crystallogr* 1953;6:689–97.
- [45] Fleishman SJ, Ben-Tal N. A novel scoring function for predicting the conformations of tightly packed pairs of transmembrane alpha-helices. *J Mol Biol* 2002;321:363–78.
- [46] Eckert R. Road to clinical efficacy: challenges and novel strategies for antimicrobial peptide development. *Future Microbiol* 2011;6:635–51.
- [47] Giuliana A, Pirri G, Nicoletto SF. Antimicrobial peptides: an overview of a promising class of therapeutics. *Cent Eur J Biol* 2007;2:1–33.
- [48] Jean-Francois F, Khemtemourian L, Odaert B, Castano S, Grelard A, Manigand C, et al. Variability in secondary structure of the antimicrobial peptide Cateslytin in powder, solution, DPC micelles and at the air-water interface. *Eur Biophys J* 2007;36:1019–27.
- [49] Das N, Murray DT, Cross TA. Lipid bilayer preparations of membrane proteins for oriented and magic angle spinning solid state NMR samples. *Nat Protoc* 2013;11:2256–70.
- [50] Gor'kov PL, Chekmenev EY, Li C, Cotten M, Buffy JJ, Traaseth NJ, et al. Using low-E resonators to reduce RF heating in biological samples for static solid-state NMR up to 900 MHz. *J Magn Reson* 2007;185:77–93.
- [51] Wu CH, Ramamoorthy A, Gierasch LM, Opella SJ. Simultaneous characterization of the amide ¹H chemical shift, ¹H-¹⁵N dipolar, and ¹⁵N chemical shift interaction tensors in a peptide bond by three-dimensional solid-state NMR spectroscopy. *J Am Chem Soc* 1995;117:6148–9.
- [52] Ramamoorthy A, Wu CH, Opella SJ. Three-dimensional solid-state NMR experiment that correlates the chemical shift and dipolar coupling frequencies of two heteronuclei. *J Magn Reson B* 1995;107:88–90.
- [53] Kim S, Cross TA. Uniformity, ideality, and hydrogen bonds in transmembrane alpha-helices. *Biophys J* 2002;83:2084–95.
- [54] Page RC, Kim S, Cross TA. Transmembrane helix uniformity examined by spectral mapping of torsion angles. *Structure* 2008;16:787–97.
- [55] Fajer PG, Brown L, Song L. Practical pulsed dipolar EPR (DEER). In: Hemminga MA, Berliner L, editors. *ESR spectroscopy in membrane biophysics*; 2007. p. 95–128.
- [56] Finiguerra MG, Prudencio M, Ubbink M, Huber M. Accurate long-range distance measurements in a doubly spin-labeled protein by a four-pulse, double electron-electron resonance method. *Magn Reson Chem* 2008;46:1096–101.
- [57] Schwieters CD, Kuszewski JJ, Tjandra N, Clore GM. The Xplor-NIH NMR molecular structure determination package. *J Magn Reson* 2003;160:65–73.
- [58] Mackerell AD, Feig M, Brooks CL. Extending the treatment of backbone energetics in protein force fields: limitations of gas-phase quantum mechanics in reproducing protein conformational distributions in molecular dynamics simulations. *J Comput Chem* 2004;25:1400–15.
- [59] Sale K, Song L, Liu YS, Perozo E, Fajer P. Explicit treatment of spin labels in modeling of distance constraints from dipolar EPR and DEER. *J Am Chem Soc* 2005;127:9334–5.
- [60] Phillips JC, Braun R, Wang W, Gumbart J, Tajkhorshid E, Villa E, et al. Scalable molecular dynamics with NAMD. *J Comput Chem* 2005;26:1781–802.